NJC

Accepted Manuscript

This is an *Accepted Manuscript*, which has been through the Royal Society of Chemistry peer review process and has been accepted for publication.

Accepted Manuscripts are published online shortly after acceptance, before technical editing, formatting and proof reading. Using this free service, authors can make their results available to the community, in citable form, before we publish the edited article. We will replace this *Accepted Manuscript* with the edited and formatted *Advance Article* as soon as it is available.

You can find more information about *Accepted Manuscripts* in the Information for Authors.

Please note that technical editing may introduce minor changes to the text and/or graphics, which may alter content. The journal's standard Terms & Conditions and the Ethical guidelines still apply. In no event shall the Royal Society of Chemistry be held responsible for any errors or omissions in this *Accepted Manuscript* or any consequences arising from the use of any information it contains.

ROYAL SOCIETY OF CHEMISTRY

www.rsc.org/njc

Journal Name

ARTICLE

Gold nanoparticles modified magnetic fibrous silica microsphere as a highly efficient and recyclable catalyst for the reduction of 4-nitrophenol

Received 00th January 20xx,
Accepted 00th January 20xx

DOI: 10.1039/x0xx00000x

www.rsc.org/

Zhengping Dong*, Guiqin Yu, Xuanduong Le

Recently, catalysts with easily accessible active sites and high efficiency and recyclability have triggered various research interests. In this study, we prepared uniform fibrous silica microspheres with a γ-Fe_2O_3 magnetic core (γ-Fe_2O_3@SiO_2@KCC-1) as the catalyst support. The distance between two fibers was approximately 10–20 nm. Au nanoparticles (NPs) were highly dispersed on the silica fibers without aggregation to form the nanocatalyst Au/γ-Fe_2O_3@SiO_2@KCC-1. The catalytic activity of Au/γ-Fe_2O_3@SiO_2@KCC-1 for the reduction of 4-nitrophenol (4-NP) with $NaBH_4$ was measured by UV-vis spectroscopy. Au/γ-Fe_2O_3@SiO_2@KCC-1 exhibited better catalytic activity toward the reduction of 4-NP compared with other reported Au NPs-based catalysts. The high catalytic activity was mainly attributed to the easy accessibility of the Au NPs of the prepared nanocatalyst. In addition, Au/γ-Fe_2O_3@SiO_2@KCC-1 could be easily recycled by applying an external magnetic field while maintaining the catalytic activity without significant decrease even after six runs. The unique properties provided an ideal platform to study various noble metal/γ-Fe_2O_3@SiO_2@KCC-1 nanocatalysts that can be potentially applied in a wide variety of fields such as catalysis and green chemistry.

1. Introduction

During the past few years, significant research progress has been made with noble metal nanoparticles (NMNPs) because of their excellent properties in many fields, especially in catalysis.[1-3] In particular, NMNPs-based catalysts have been extensively studied in many organic catalytic reactions, including cross coupling, hydrogenation, and methanol oxidation.[4-6] To date, various methods have been developed for preparing NMNPs-based catalysts, among which the chemical reduction of noble metal cations in a solution using a reducing reagent is the most common preparation procedure.[7-9] However, in solution, NMNPs are unstable and tend to aggregate because of their high surface energy resulting from the high surface-to-volume ratio, which in turn leads to a remarkable reduction in the catalytic activity.[10, 11] To solve this problem, NMNPs have been grafted onto various supporting matrices to generate hybrid catalysts to protect against the aggregation of NMNPs. Among most of the reported supporting materials, mesoporous silicas such as SBA-15, SBA-16, MCM-41, MCM-48, and other mesoporous silica microspheres have been widely used to fabricate NMNPs-based nanocatalysts.[8, 12-16] Although these mesoporous silicas have regular mesopores and high specific surface areas that can support NMNPs with high dispersion, their mesopores can always be easily blocked because of the small pore size. For example, by using cetyltrimethylammonium bromide as the surfactant, the prepared mesoporous silicas usually exhibit a pore size of 2–5 nm,[17, 18] while the particle size of most of the NMNPs is 3–5 nm. Thus, designing silica supports with a large pore size and easily accessible high surface areas is required. Furthermore, the isolation and recovery of NMNPs-based catalysts from the catalytic reaction medium with high efficiency is also worthy of consideration due to the scarcity of noble metal resources. In this regard, magnetic-responsive nanomaterials have emerged as ideal catalyst supports since they can be isolated and recovered by magnetic separation, which is more efficient and rapid as compared with centrifugation or filtration, which prevents mass losses of catalyst or the use of additional solvents.[19-23] Therefore, it is highly desirable to prepare magnetic silica materials with easy accessible high surface areas, high-efficiency mass transfer, as well as magnetic separation property, to further fabricate NMNPs-based catalysts for organic catalytic reactions.

On the other hand, 4-nitrophenol (4-NP) and related compounds are organic pollutants present in industrial and agricultural wastewaters as these compounds are primarily used to prepare dyes, pesticides, explosives, plasticizers, and herbicides.[24-26] Hence, to meet increasingly stringent environmental quality standards, it is necessary to remove them from polluted waters.[11, 27] Among all the processes to remove 4-NP, the catalytic reduction of 4-NP to 4-aminophenol (4-AP) is the most efficient because it is cost-effective and simple. In addition, 4-AP is formed as the reduction product, which is an industrially important raw material widely used as the intermediate for the manufacture of many analgesic and antipyretic drugs.[28, 29] Thus far, various NMNPs-based catalysts such as Pd, Au,

College of Chemistry and Chemical Engineering, Gansu Provincial Engineering Laboratory for Chemical Catalysis, Lanzhou University, Lanzhou 730000, PR China. E-mail: dongzhp@lzu.edu.cn; Fax: +86 0931 8912582; Tel: +86 0931 8912577.

Ag, and Pt nanocatalysts have been widely used for the reduction of 4-NP to 4-AP due to their efficient catalytic activities.[30-32] However, cost-effective NMNPs based catalysts with easily accessible active sites, excellent catalytic activities, and efficient recoverable properties for the reduction of 4-NP to 4-AP are still needed.

Inspired by the abovementioned perspective, herein, we prepared uniform fibrous silica microspheres (KCC-1) with a γ-Fe_2O_3 magnetic core as the catalyst support (γ-Fe_2O_3@SiO_2@KCC-1) for the immobilization of NMNPs. The silica fibers were functionalized with mercaptopropyl groups followed by the immobilization of Au NPs onto the fibers without aggregation. Besides, the large space between fibers can significantly increase the accessibility of the active sites of the prepared nanocatalyst. In addition, the catalytic performance of Au/γ-Fe_2O_3@SiO_2@KCC-1 with respect to efficiency and recyclability was also evaluated for the reduction of 4-NP in the presence of $NaBH_4$.

2. Experimental

2.1 Materials

In this study, the starting reagents tetraethoxysilane (TEOS), 3-mercaptopropyltrimethoxysilane (MPTES), cetylpyridinium bromide (CPB), sodium dodecyl sulfate (SDS), glycol, urea, ferric trichloride ($FeCl_3 \cdot 6H_2O$), chloroauric acid ($HAuCl_4$), and anhydrous sodium acetate (NaAc) were commercially obtained from Shanghai Chemical Company (Shanghai, China) and used as received. Reagent-grade 4-NP, cyclohexane, pentanol, and $NaBH_4$ were purchased from Tianjing Guangfu Chemical Company (Tianjin, China). All reagents and solvents used for synthesis and measurements were used as supplied.

2.2 Preparation of Fe_3O_4 NPs

Fe_3O_4 magnetic NPs were synthesized according to the reported literature.[18, 33] Typically, $FeCl_3 \cdot 6H_2O$ (2.7 g), SDS (1.0 g), and NaAc (7.2 g) were mixed in 100 mL of glycol and stirred at room temperature for 30 min. Then, the solution was poured into a Teflon flask and aged at 200 °C for 8 h. After being cooled, the solid product was filtered and thoroughly washed with deionized water to obtain Fe_3O_4 NPs.

2.3 Fabrication of γ-Fe_2O_3@SiO_2@KCC-1

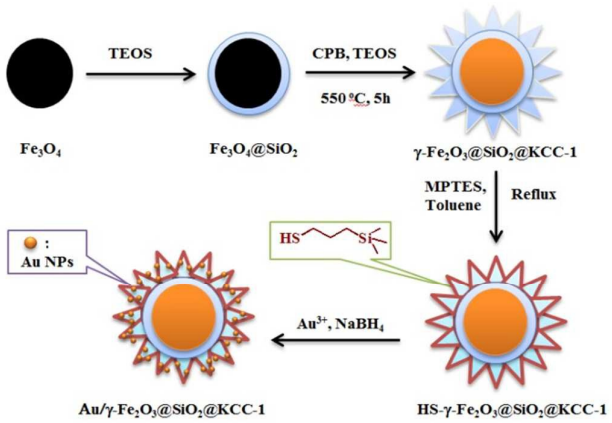

Scheme 1. Preparation of Au/γ-Fe_2O_3@SiO_2@KCC-1

First, the Fe_3O_4 NPs were covered by amorphous silica (Fe_3O_4@SiO_2) to allow further growth of fibrous nano-silica. Typically, 0.5 g of fresh Fe_3O_4 NPs was dispersed in 200 mL of ethanol, 50 mL of deionized water, and 2.5 mL of concentrated ammonia and ultrasonicated for 30 min. Second, 0.5 g of TEOS was added dropwise. The mixture was stirred at room temperature for 5 h. Then, the resulting solid product was separated by magnetic suction and thoroughly washed with deionized water and ethanol.

According to the preparation method of fibrous nano-silica KCC-1,[34-36] the core–shell magnetic fibrous silica microspheres were prepared as follows: the above obtained Fe_3O_4@SiO_2 (0.25 g) was ultrasonically dispersed in an aqueous solution (30 mL) containing urea (0.3 g) to form solution A. CPB (0.5 g) was added to 0.75 mL of n-pentanol and 30 mL cyclohexane to form solution B. Solution A was added to solution B under stirring at room temperature. Then, 1.25 g TEOS was added dropwise to the above mixed solution. The resulting mixture was continuously stirred for 1 h at room temperature and then aged at 120 °C for 5 h. Then, the mixture was allowed to cool to room temperature and isolated by strong magnetic suction, washed with deionized water and acetone, and dried overnight in a drying oven at 40 °C overnight. The obtained material was then calcined at 550 °C for 5 h in air to obtain γ-Fe_2O_3@SiO_2@KCC-1.

2.4 Preparation of Au/γ-Fe_2O_3@SiO_2@KCC-1 nanocatalyst

γ-Fe_2O_3@SiO_2@KCC-1 was functionalized with MPTES prior to the immobilization of Au NPs onto the fibrous nano-silica. First, γ-Fe_2O_3@SiO_2@KCC-1 (0.3 g) was added to 30 mL of anhydrous toluene under ultrasonication for 10 min to disperse it homogeneously. Second, 30 mg of MPTES was added dropwise, and the mixture was refluxed for 5 h in a N_2 atmosphere. Next, the mixture was cooled to room temperature, and the resulting mercaptopropyl-functionalized material (HS-γ-Fe_2O_3@SiO_2@KCC-1) was magnetically isolated, washed repeatedly with chloroform, dichloromethane, and ethanol, and dried under vacuum.

HS-γ-Fe_2O_3@SiO_2@KCC-1 (0.1 g) was ultrasonically dispersed in 10 mL H_2O, and 5 mL of an $HAuCl_4$ solution containing 5 mg Au was added. After being stirred and ultrasonically dispersed for 1 h, an excess of a $NaBH_4$ solution was added dropwise. Then, the Au NPs were formed and anchored on the mercaptopropyl-functionalized fibrous silica. Thus, the Au/γ-Fe_2O_3@SiO_2@KCC-1 nanocatalyst was obtained.

2.5 Procedure for the reduction of 4-NP

For the catalytic reduction of 4-NP, a 4-NP aqueous solution (0.01 M, 30 μL) was first mixed with H_2O (2.7 mL) and then a freshly prepared aqueous $NaBH_4$ solution (0.1 M, 0.25 mL) was added, which resulted in the formation of a bright yellow solution. Then, the prepared Au/γ-Fe_2O_3@SiO_2@KCC-1 nanocatalyst (10 μL, 20 mg mL^{-1}) was added to the bright yellow solution, and the reaction was continued until the solution became colorless. The progress of the reduction process was monitored by measuring the ultraviolet–visible (UV–vis) absorption spectra from 250 nm to 500 nm. To investigate the reusability of the nanocatalyst, the reduction reaction was amplified 20 times, and a magnet was used to recover the nanocatalyst for the next catalytic run.

2.6 Characterization

Transmission electron microscopy (TEM, Tecnai G2F30) was used to investigate the size and morphology of the prepared samples. X-ray diffraction measurements were performed on a diffractometer (XRD, Rigaku D/max-2400) using Cu-Kα radiation as the X-ray source in the 2θ range of 10–80°. X-ray photoelectron spectroscopy (XPS, PHI-5702) was employed, and the C 1S line at 284.6 eV was used as the binding energy reference. Magnetic measurements of γ-Fe_2O_3@SiO_2@KCC-1 and Au/γ-Fe_2O_3@SiO_2@KCC-1 were performed using a vibrating sample magnetometer (VSM, Quantum Design) at room temperature in an applied magnetic field sweeping from −10 to 10 kOe. A Fourier transform infrared spectrometer (FTIR, Bruker IFS66/S) was used to obtain the FTIR spectra of γ-Fe_2O_3@SiO_2@KCC-1 and HS-γ-Fe_2O_3@SiO_2@KCC-1. Elemental analysis (Gmbh Vario El Elementar) and inductively coupled plasma (ICP-AES, IRIS Advantage analyzer) were employed to measure the S, C, H, and Au content of the samples. A UV–Vis spectrophotometer (Shimadzu UV 2100 PC) was used to collect the absorption data.

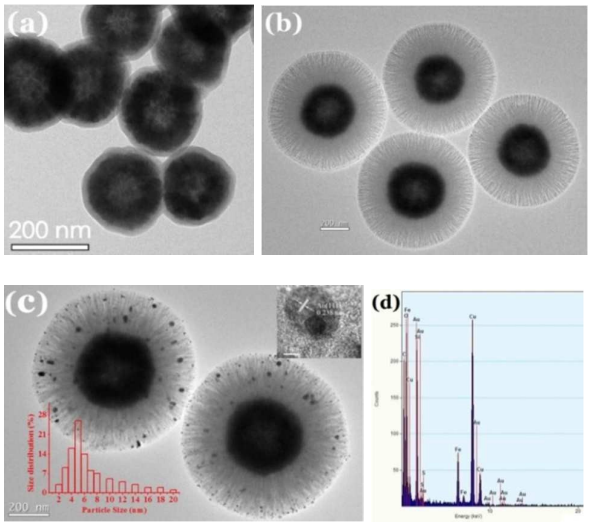

Fig. 1. (a) TEM of Fe_3O_4@SiO_2, (b) TEM of γ-Fe_2O_3@SiO_2@KCC-1, (c) TEM of Au/γ-Fe_2O_3@SiO_2@KCC-1 and (d) EDX spectra of Au/γ-Fe_2O_3@SiO_2@KCC-1.

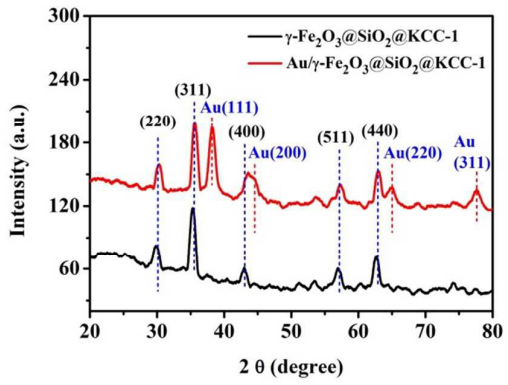

Fig. 2. XRD patterns of γ-Fe_2O_3@SiO_2@KCC-1 and Au/γ-Fe_2O_3@SiO_2@KCC-1.

3. Results and discussion

Scheme 1 shows the schematic of preparing the Au/γ-Fe_2O_3@SiO_2@KCC-1 nanocatalyst. Frist, γ-Fe_2O_3@SiO_2@KCC-1 was functionalized with MPTES to form mercaptopropyl-functionalized material (HS-γ-Fe_2O_3@SiO_2@KCC-1). The mercaptopropyl groups on the fibrous silica acted as adsorption centers for Au^{3+}. When $NaBH_4$ was introduced, the Au^{3+} ions were reduced and immobilized onto the fibers of γ-Fe_2O_3@SiO_2@KCC-1.

3.1 Catalyst characterization

In the preparation of γ-Fe_2O_3@SiO_2@KCC-1, Fe_3O_4 NPs were covered by amorphous silica to form Fe_3O_4@SiO_2 (black powder, Fig. S1a) to allow for the further growth of fibrous nano-silica. When the as-synthesized material was calcined at 550 °C for 5 h in air, the Fe_3O_4 NPs in the core were converted into magnetic γ-Fe_2O_3 as previously reported,[37, 38] resulting in the formation of γ-Fe_2O_3@SiO_2@KCC-1 (brown powder, Fig. S1b). Fe_3O_4@SiO_2 has a near spherical morphology with a Fe_3O_4 core of approximately 160 nm and a SiO_2 shell of approximately 20 nm (Fig. 1a). When covered with fibrous nano-silica, the diameter of the NPs increased to 600 nm, and the morphology was uniform microspheres with fibrous nano-silica on the surface (Fig. 1b). To easily load the Au NPs on the fibrous nano-silica, γ-Fe_2O_3@SiO_2@KCC-1 was then functionalized with MPTES. As displayed in the FTIR spectra (Fig. S2), the absorption peak at 2920 cm^{-1} corresponded to –CH stretching, indicating the successful grafting of mercaptopropyl groups on the γ-Fe_2O_3@SiO_2@KCC-1 surface. As measured by elemental analysis, the mercaptopropyl group content was approximately 4.5% (Table S1). The distance between two fibers was approximately 10–20 nm. This large distance permits the easy loading of the Au NPs onto fibrous nano-silica. Fig. 1c shows the TEM image of Au/γ-Fe_2O_3@SiO_2@KCC-1. The Au NPs with an average diameter of approximately 5 nm (*Fig. 1c, inset*) were remarkably grafted on the fibers of the γ-Fe_2O_3@SiO_2@KCC-1 microspheres, and no obvious aggregation was observed. The lattice fringe with a spacing of 0.238 nm corresponded to the Au(111) planes (Fig. 1c, inset). Energy-dispersive spectroscopy (EDX) analysis clearly shows the chemical composition of Au/γ-Fe_2O_3@SiO_2@KCC-1 (Fig. 1d). Furthermore, ICP-AES analysis revealed that the content of Au NPs loaded on the surface of γ-Fe_2O_3@SiO_2@KCC-1 was approximately 4.63% (Table S1).

XRD measurements were conducted to confirm the surface composition of the prepared samples (Fig. 2). Characteristic peaks of (220), (311), (400), (511), and (440) were observed for γ-Fe_2O_3@SiO_2@KCC-1, which are typical of a spinel magnetite structure of γ-Fe_2O_3.[39, 40] After modifying by Au NPs, the characteristic peaks of γ-Fe_2O_3 were still preserved. However, compared with the XRD pattern of γ-Fe_2O_3@SiO_2@KCC-1, that of Au/γ-Fe_2O_3@SiO_2@KCC-1 exhibited four characteristic peaks at 2θ = 38, 44, 65, and 78°, corresponding to the (111), (200), (220), and (311) lattice planes of Au, respectively (JCPDS, No. 4-0784). These results indicated that the Au NPs are successfully immobilized onto the fibers of the γ-Fe_2O_3@SiO_2@KCC-1 microspheres.

To examine the valence states of Au NPs, XPS analysis was conducted; the results are shown in Fig. 3. As shown in Fig. 3a, the XPS elemental survey scan of Au/γ-Fe_2O_3@SiO_2@KCC-1 clearly revealed the presence of Si, O, C as well as Au elements in the

sample. A very weak peak was observed for the Fe element because γ-Fe_2O_3 was in the core of the microsphere. Using the C 1S line at 284.6 eV as the binding energy reference (Fig. 3b), the peaks at 710.6 and 724.3 eV were assigned to Fe $2p_{3/2}$ and Fe $2p_{1/2}$, respectively (Fig. 3c). Two obvious Au 4f peaks were observed in Fig. 3d, which are indicative of metallic Au at binding energies of 83.8 and 87.4 eV in Au $4f_{7/2}$ and Au $4f_{5/2}$ levels, respectively.

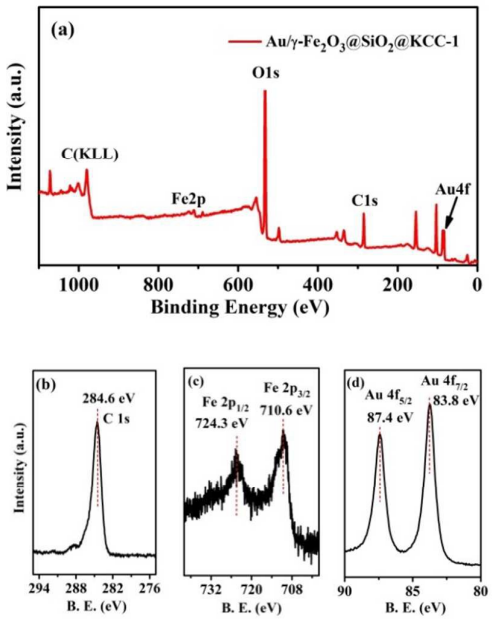

Fig. 3. XPS wide-scan spectra of Au/γ-Fe_2O_3@SiO_2@KCC-1 (a), C 1s (b), Fe 2p (c) and Au 4f (d).

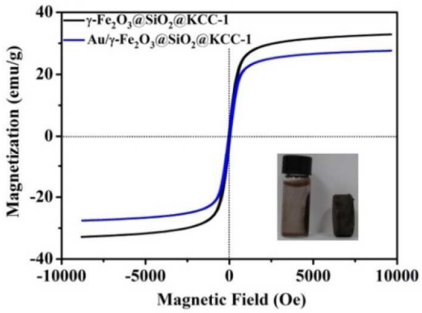

Fig. 4. Room temperature magnetization curves of γ-Fe_2O_3@SiO_2@KCC-1 and Au/γ-Fe_2O_3@SiO_2@KCC-1.

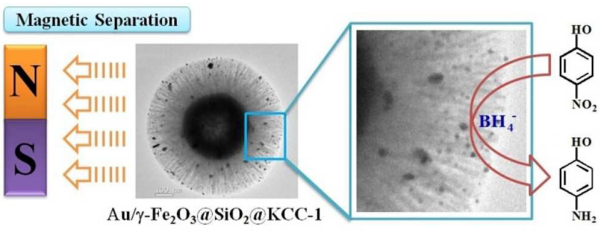

Scheme 2. Reduction of 4-NP to 4-AP over Au/γ-Fe_2O_3@SiO_2@KCC-1 and the catalyst recycle procedure.

The magnetic behavior of Au/γ-Fe_2O_3@SiO_2@KCC-1 that was essential for magnetic applications was evaluated through magnetic measurements conducted at room temperature (Fig. 4). The measured saturation magnetization (Ms) value of γ-Fe_2O_3@SiO_2@KCC-1 was 32.8 emu g^{-1}. When loaded with Au NPs, the magnetic saturation values reduced to 27.6 emu g^{-1}. Thus, Au/γ-Fe_2O_3@SiO_2@KCC-1 could be efficiently separated from the reaction mixture by an external magnetic force and reused (Fig. 4, inset).

3.2 Catalytic reduction of 4-NP

The catalytic performance of Au/γ-Fe_2O_3@SiO_2@KCC-1 was evaluated by the catalytic reduction of 4-NP with an excess of $NaBH_4$ (Scheme 2). Here, reaction conditions of room temperature and distilled water were chosen to ensure an energy saving and environmentally friendly reaction.[41]

As shown in Fig. 5a, the 4-NP aqueous solution with light yellow color exhibited a typical absorption peak at 317 nm. When a $NaBH_4$ solution was added, the 4-NP aqueous solution changed to bright yellow, and the absorption peak red-shifted to 400 nm, corresponding to the formation of 4-nitrophenolate in alkaline conditions.[42] The peak at 400 nm remained unaltered with time, suggesting that reduction does not occur in the absence of a catalyst as previously reported.[43] The addition of Au/γ-Fe_2O_3@SiO_2@KCC-1 (Fig. 5b) to 4-NP led to the decrease in the peak intensity of the 4-nitrophenolate ion at 400 nm with a concomitant increase in the peaks corresponding to 4-AP at 300 nm, reflecting the conversion of 4-NP to 4-AP.

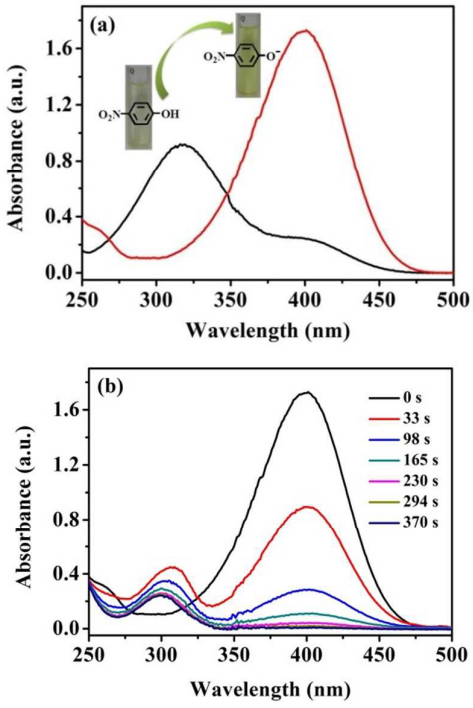

Fig. 5. (a) UV-Vis spectra of 4-NP before and after adding $NaBH_4$ solution and (b) successive UV-vis spectra for the reduction of 4-NP by $NaBH_4$ with Au/γ-Fe_2O_3@SiO_2@KCC-1.

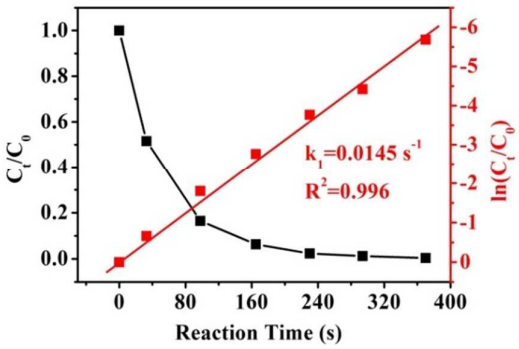

Fig. 6. Kinetic curve for the reduction of 4-NP catalyzed by Au/γ-Fe_2O_3@SiO_2@KCC-1 (C_t and C_0 are 4-NP concentrations at time t and 0, respectively).

The reaction proceeded rapidly and was almost completed in 6 min catalyzed by Au/γ-Fe_2O_3@SiO_2@KCC-1. The conversion of 4-NP was calculated from the C_t/C_0 ratio, where C_0 and C_t represent the concentration of 4-NP at time 0 and t, respectively, and it was measured from the relative intensity of the absorbance (A_t/A_0) at 400 nm. After the completion of the reaction, the reaction mixture became colorless. According to the traditional theory about the catalytic reduction of 4-NP by metal NPs, the catalytic mechanism was described as follows: when BH_4^- ions and 4-NP molecules are adsorbed onto the catalytic centers, electron transfer occurs from BH_4^- to 4-NP, resulting in the reduction of 4-NP.[43]

The reduction rate can be assumed to be independent of $NaBH_4$ because when the initial concentration of the $NaBH_4$ solution is very high, it can be considered constant throughout the whole reduction process. Thus, the reaction can be considered as a pseudo-first-order reaction with regard to 4-NP only to evaluate the catalytic rate.[24] The apparent rate constant k_{app} can be defined as [Eq. (1)]:

$$\ln\left(\frac{C_t}{C_0}\right) = \ln\left(\frac{A_t}{A_0}\right) = -K_{app}t \qquad (1)$$

Using the above equation [Eq. (1)], a linear relationship between $\ln(C_t/C_0)$ and reaction time was obtained for the reduction catalyzed by Au/γ-Fe_2O_3@SiO_2@KCC-1 (Fig. 6), which matches well with the first-order reaction kinetics. The reaction rate constant K_{app} was calculated to be 1.45×10^{-2} s^{-1} for the reduction reaction catalyzed by Au/γ-Fe_2O_3@SiO_2@KCC-1 (Fig. 6).

However, it is not entirely reasonable to compare k_{app} of different supported catalysts because the metal loadings were different. To further compare the catalytic activity of Au/γ-Fe_2O_3@SiO_2@KCC-1 with other reported catalysts, the rate constant per gram active sites was then calculated [Eq. (2)]:

$$K_M = \frac{K_{app}}{M} \qquad (2)$$

where M is the weight of active sites used.[48, 49] Based on the amount of catalyst used and the ICP-AES data (Table S1), the activity parameter K_M was calculated to be 1565.9 s^{-1} g^{-1} for the reduction reaction catalyzed by Au/γ-Fe_2O_3@SiO_2@KCC-1 (Fig. 6).

The catalytic activities of Au/γ-Fe_2O_3@SiO_2@KCC-1 and other NMNPs loaded on different supports were compared for the reduction of 4-NP; these results are listed in Table 1. Our group previously reported that a Au/magnetic porous carbon (Au/MPC) nanocatalyst exhibited an activity parameter of 848.2 s^{-1} g^{-1} for the reduction of 4-NP,[44] while the K_M values for the reported Au/graphene catalyst and carbon@Au core–shell nanofiber catalyst were 132.08 and 238.98 s^{-1} g^{-1}, respectively.[45, 46] For the reported Pd NPs-based catalyst Pd/PPy, the activity parameter K_M was approximately 1400 s^{-1} g^{-1}.[47] Thus, Au/γ-Fe_2O_3@SiO_2@KCC-1 with the activity parameter K_M of 1565.9 s^{-1} g^{-1} exhibits excellent catalytic activity, which is mainly attributed to the ease of access of active sites and the low aggregation of the Au NPs on the γ-Fe_2O_3@SiO_2@KCC-1 support. In this situation, mass transfer has been dramatically enhanced, and both 4-NP and BH_4^- can be easily adsorbed on the Au NPs surface, which allows the reduction to start and end rapidly.

Furthermore, the stability and recyclability of the catalyst is an important issue. After each catalytic cycle, Au/γ-Fe_2O_3@SiO_2@KCC-1 was quantitatively separated from the reaction mixture using an external magnet as described in Fig. 4. The spent catalyst was then thoroughly washed in turn with water and ethanol and reused in subsequent runs under identical reaction conditions. As displayed in Fig. 7, Au/γ-Fe_2O_3@SiO_2@KCC-1 could be successfully recycled and reused for at least six times with stable conversion above 96% within 6 min in the reduction of 4-NP.

Table 1. Comparison of the catalytic activity for the reduction of 4-NP between Au/γ-Fe_2O_3@SiO_2@KCC-1 and some catalysts reported in the literature.

Samples	Catalyst used (mg)	NMNPs loading (wt%)	K_{app} (s^{-1})	K_M (s^{-1} g^{-1})
Au/MPC[44]	0.3	3.93	1×10^{-2}	848.2
Au/graphene[45]	0.1	24	3.17×10^{-3}	132.08
carbon@Au[46]	0.1	22.68	5.42×10^{-3}	238.98
Pd/PPy[47]	0.0125	50.2	8.87×10^{-3}	1413
This work	0.2	4.63	1.45×10^{-2}	1565.9

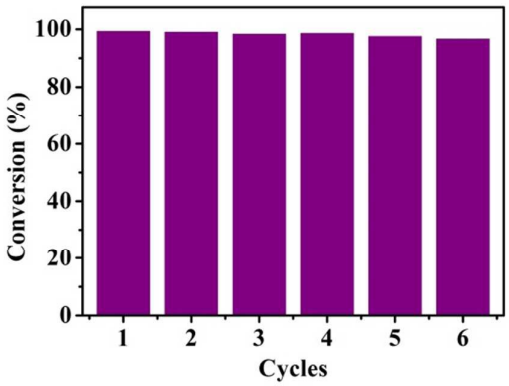

Fig.7. The reusability of Au/γ-Fe_2O_3@SiO_2@KCC-1 for the reduction of 4-NP with $NaBH_4$.

4. Conclusions

In conclusion, the Au/γ-Fe_2O_3@SiO_2@KCC-1 nanocatalyst was prepared by modifying uniform magnetic fibrous silica microspheres γ-Fe_2O_3@SiO_2@KCC-1 with Au NPs. The as-prepared Au/γ-Fe_2O_3@SiO_2@KCC-1 nanocatalyst exhibited higher catalytic activity for the reduction of 4-NP to 4-AP as compared with other reported Au NPs-based catalysts, probably caused by the easy accessibility of the Au active sites. Au/γ-Fe_2O_3@SiO_2@KCC-1 can also be easily recycled and reused, which is attributed to its superparamagnetic property. We believe that these results will be beneficial for improving catalytic activity and recyclability to develop advanced noble-metal-based catalysts.

Acknowledgments

The authors acknowledge financial support from the NSFC (Grants 21301082) and the Fundamental Research Funds for the Central Universities (lzujbky-2015-21 and lzujbky-2015-32).

Notes and references

1. L. Shi, M. Liu, L. Liu, W. Gao, M. Su, Y. Ge, H. Zhang and B. Dong, *Langmuir*, 2014, **30**, 13456-13461.
2. S. Akbayrak, M. Kaya, M. Volkan and S. Özkar, *Appl. Catal. B: Environ.*, 2014, **147**, 387-393.
3. T. Mitsudome, Y. Takahashi, T. Mizugaki, K. Jitsukawa and K. Kaneda, *Angew. Chem. Int. Edit.*, 2014, **53**, 8348-8351.
4. S.-B. Wang, W. Zhu, J. Ke, M. Lin and Y.-W. Zhang, *ACS Catal.*, 2014, **4**, 2298-2306.
5. S. K. Das, T. Parandhaman, N. Pentela, A. K. M. Maidul Islam, A. B. Mandal and M. Mukherjee, *J. Phys. Chem. C*, 2014, **118**, 24623-24632.
6. E. A. Franceschini, G. A. Planes, F. J. Williams, G. J. A. A. Soler-Illia and H. R. Corti, *J. Power Sources*, 2011, **196**, 1723-1729.
7. J. Sun, Y. Fu, G. He, X. Sun and X. Wang, *Appl. Catal. B: Environ.*, 2015, **165**, 661-667.
8. K. Nakatsuka, K. Mori, S. Okada, S. Ikurumi, T. Kamegawa and H. Yamashita, *Chem. Eur. J.*, 2014, **20**, 8348-8354.
9. L. Gao, T. Nishikata, K. Kojima, K. Chikama and H. Nagashima, *Chem. Asian J.*, 2013, **8**, 3152-3163.
10. Z. Wang, H. Fu, D. Han and F. Gu, *J. Mater. Chem. A*, 2014, **2**, 20374-20381.
11. Y. Tian, Y.-y. Cao, F. Pang, G.-q. Chen and X. Zhang, *Rsc Adv.*, 2014, **4**, 43204-43211.
12. N. Anand, P. Ramudu, K. H. P. Reddy, K. S. R. Rao, B. Jagadeesh, V. S. P. Babu and D. R. Burri, *Appl. Catal. A: General*, 2013, **454**, 119-126.
13. W. J. Yu, Y. Tang, L. Y. Mo, P. Chen, H. Lou and X. M. Zheng, *Catal. Commun.*, 2011, **13**, 35-39.
14. Z. C. Ma, H. Q. Yang, Y. Qin, Y. J. Hao and G. A. Li, *J. Mol. Catal. a-Chem.*, 2010, **331**, 78-85.
15. S. Banerjee, V. Balasanthiran, R. T. Koodali and G. A. Sereda, *Org. Biomol. Chem.*, 2010, **8**, 4316-4321.
16. Y. Zhang, E. C. Judkins, D. R. McMillin, D. Mehta and T. Ren, *ACS Catal.*, 2013, **3**, 2474-2478.
17. W. Li, B. L. Zhang, X. J. Li, H. P. Zhang and Q. Y. Zhang, *Appl. Catal. A: General*, 2013, **459**, 65-72.
18. Y. Wang, B. Li, L. Zhang, P. Li, L. Wang and J. Zhang, *Langmuir*, 2012, **28**, 1657-1662.
19. M. Rocha, C. Fernandes, C. Pereira, S. L. H. Rebelo, M. F. R. Pereira and C. Freire, *Rsc Adv.*, 2015, **5**, 5131-5141.
20. J. Yoo, N. Park, J. H. Park, J. H. Park, S. Kang, S. M. Lee, H. J. Kim, H. Jo, J.-G. Park and S. U. Son, *ACS Catal.*, 2015, **5**, 350-355.
21. B. Karimi, F. Mansouri and H. Vali, *Green. Chem.*, 2014, **16**, 2587-2596.
22. Z. Dong, K. Liang, C. Dong, X. Li, X. Le and J. Ma, *Rsc Adv.*, 2015, **5**, 20987-20991.
23. Z. Dong, X. Le, C. Dong, W. Zhang, X. Li and J. Ma, *Appl. Catal. B: Environ.*, 2015, **162**, 372-380.
24. Y. Yang, Y. Zhang, C. J. Sun, X. Li, W. Zhang, X. Ma, Y. Ren and X. Zhang, *Chemcatchem*, 2014, **6**, 3084-3090.
25. S. Zhang, S. Gai, F. He, Y. Dai, P. Gao, L. Li, Y. Chen and P. Yang, *Nanoscale*, 2014, **6**, 7025-7032.
26. Z. Dong, X. Le, X. Li, W. Zhang, C. Dong and J. Ma, *Appl. Catal. B: Environ.*, 2014, **158–159**, 129-135.
27. V. K. Gupta, I. Ali, T. A. Saleh, A. Nayak and S. Agarwal, *Rsc Adv.*, 2012, **2**, 6380-6388.
28. Z. Niu, S. Zhang, Y. Sun, S. Gai, F. He, Y. Dai, L. Li and P. Yang, *Dalton Trans.*, 2014, **43**, 16911-16918.
29. A. Shukla, R. K. Singha, T. Sasaki and R. Bal, *Green Chem.*, 2015, **17**, 785-790.
30. J.-J. Lv, A.-J. Wang, X. Ma, R.-Y. Xiang, J.-R. Chen and J.-J. Feng, *J. Mater. Chem. A*, 2015, **3**, 290-296.
31. W. Wu, M. Lei, S. Yang, L. Zhou, L. Liu, X. Xiao, C. Jiang and V. A. L. Roy, *J. Mater. Chem. A*, 2015, **3**, 3450-3455.
32. C. Chu and Z. Su, *Langmuir*, 2014, **30**, 15345-15350.
33. L. Bing, *Sens. Actuators B*, 2014, **198**, 342-349.
34. V. Polshettiwar, D. Cha, X. Zhang and J. M. Basset, *Angew. Chem. Int. Edit.*, 2010, **49**, 9652-9656.
35. A. Fihri, D. Cha, M. Bouhrara, N. Almana and V. Polshettiwar, *Chemsuschem*, 2012, **5**, 85-89.
36. A. Fihri, M. Bouhrara, U. Patil, D. Cha, Y. Saih and V. Polshettiwar, *ACS Catal.*, 2012, **2**, 1425-1431.
37. X. Li, X.-H. Zhu, Y. Fang, H.-L. Yang, X. Zhou, W. Chen, L. Jiao, H. Huo and R. Li, *J. Mater. Chem. A*, 2014, **2**, 10485-10491.
38. Z. Zhang, J. Zhen, B. Liu, K. Lv and K. Deng, *Green Chem.*, 2015, **17**, 1308-1317.
39. J. Yang, H. Zhang, M. Yu, I. Emmanuelawati, J. Zou, Z. Yuan and C. Yu, *Adv. Funct. Mater.*, 2014, **24**, 1354-1363.
40. Y. N. Wu, M. Zhou, S. Li, Z. Li, J. Li, B. Wu, G. Li, F. Li and X. Guan, *Small*, 2014, **10**, 2927-2936.
41. Y. Zhang, W. Yan, Z. Sun, X. Li and J. Gao, *Rsc Adv.*, 2014, **4**, 38040-38047.
42. J. Luo, N. Zhang, R. Liu and X. Liu, *Rsc Adv.*, 2014, **4**, 64816-64824.
43. Z. Jiang, D. Jiang, A. M. Showkot Hossain, K. Qian and J. Xie, *Phys. Chem. Chem. Phys.*, 2015, **17**, 2550-2559.
44. Z. Dong, X. Le, Y. Liu, C. Dong and J. Ma, *J. Mater. Chem. A*, 2014, **2**, 18775-18785.
45. J. Li, C. Y. Liu and Y. Liu, *J. Mater. Chem.*, 2012, **22**, 8426-8430.
46. P. Zhang, C. L. Shao, X. H. Li, M. Y. Zhang, X. Zhang, C. Y. Su, N. Lu, K. X. Wang and Y. C. Liu, *Phys. Chem. Chem. Phys.*, 2013, **15**, 10453-10458.
47. Y. Xue, X. Lu, X. Bian, J. Lei and C. Wang, *J. Coll. Interf. Sci.*, 2012, **379**, 89-93.
48. J. Zhang, G. Chen, M. Chaker, F. Rosei and D. Ma, *Appl. Catal. B: Environ.*, 2013, **132**, 107-115.
49. B. Baruah, G. J. Gabriel, M. J. Akbashev and M. E. Booher, *Langmuir*, 2013, **29**, 4225-4234.

Graphical Abstract

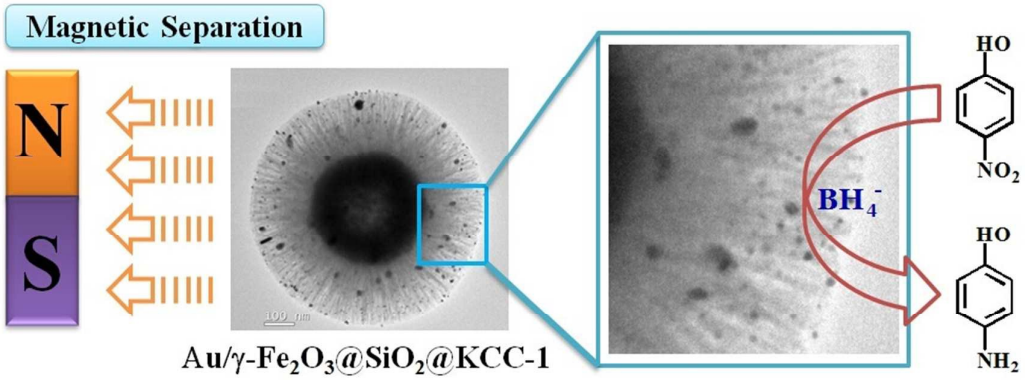

Au nanoparticles were immobilized on magnetic fibrous silica microspheres as highly activity and recyclable nanocatalyst for the catalytic reduction of 4-nitrophenol to 4-aminophenol.